DESIGN AND OPTIMIZATION OF AN INTEGRATED EXCAVATION AND TRANSPLANTING DEVICE FOR TOBACCO
/
烟草打塘-移栽一体化装置的设计与优化

Zhiguo PAN[1)], Tianfeng SUN[1)], Xiaomeng WANG*[2)], Qiuqiang HOU[2)], Shiting LV[1)], Luming ZHANG[2)], Zhenfei YANG[2)], Xuehui ZHANG[2)]

[1)]College of Mechanical and Electrical Engineering, Qingdao Agricultural University, Qingdao, 266000, China;
[2)]Yunnan Tobacco Company Honghezhou Company, Honghezhou 652300, China;
DOI: https://doi.org/10.35633/inmateh-71-34

Keywords: *Tobacco Seedling Transplantation, Conical spiral blade, Discrete Element, Simulation optimization*

ABSTRACT

To overcome inadequate functional integration, irregular pits, and insufficient agricultural machinery and agronomy in tobacco seedling transplanting equipment under film, a digging transplanting integrated machine was built. The machine uses parallel four-bar mechanism. The excavation equipment uses conical spiral blades. Using the trajectory approach, the four bar mechanism's fundamental parameters can be reversed. This method meets the requirements for coordinated excavation and transplantation. Mechanical study of soil units determines upward movement characteristics. Additionally, spiral angle, spiral blade outer diameter, and spiral blade speed are quantified to affect soil movement. The range of factors is derived. Based on three factors binary regression orthogonal combination simulated optimization experiment, a discrete element analysis was performed to enhance parameters. Experimental factors optimized include a spiral angle of 19°, a spiral blade diameter of 378 mm, and a rotational speed of 258 rpm. The two optimized test indicators are: a 193 mm hole depth and 350 mm hole diameter. The improved results were verified by field validation studies using a 191 mm hole depth and 347 mm hole diameter. The simulation optimization results and field validation experiment results are very similar. This study provides a technical basis for tobacco farming concurrent drilling and transplanting research.

摘 要

针对目前烟苗膜下移栽装备功能集成度差、打塘不规整、农机农艺融合度较差等问题，设计了一种基于平行四杆机构的打塘-移栽一体式移栽机，其中打塘装置采用锥形绞龙结构。通过轨迹法反求出四杆机构的基本参数，满足打塘和移栽的同步同穴作业。通过力学分析，确定出土壤运动过程中的临界条件，计算出影响土壤运动的主要因素包括螺旋升角、钻头外径和钻头转速，并推导出因素的范围。为优化参数，进行了基于离散元的三因素二元回归正交组合仿真优化试验。优化后的试验因素为：螺旋升角为19°、钻头外径为378mm、钻头转速为258rpm。优化后的两项试验指标的结果为：穴孔的深度为 193mm，穴孔的直径为 350mm。为验证优化后的结果进行了田间验证试验，穴孔深度为191mm，穴孔直径为347mm。田间验证试验结果与仿真优化后的结果十分接近。本研究为烟苗打塘-移栽一体机的研发提供技术参考。

INTRODUCTION

Tobacco cultivation in the southern area of China involves the transplantation of tobacco plants into meticulously excavated deep trenches. Research conducted by agronomists has demonstrated that the practice of transplanting tobacco seedlings in deep pits yields several beneficial outcomes. These include an increase in temperature, enhanced resistance to drought, preservation of soil moisture, improved lighting conditions, enhanced soil fertility, reduced incidence of pests and diseases, and the provision of a conducive environment for the early growth of tobacco seedlings *(Chen et al., 2014; Wang et al., 2010)*.

Cui conducted a series of field tests aimed at investigating the influence of deep pit dimensions, specifically the diameter and depth, on tobacco development. Through these studies, Cui effectively demonstrated the significant role that pit size plays in determining the growth of tobacco plants *(Cui et al., 2018)*. Hence, the practice of excavating deep pits in tobacco transplanting operations has a clear correlation with the overall quality of tobacco transplantation and subsequent production. In order to tackle this critical process, scholars have conducted extensive research on devices for excavating deep pits. Academic researchers have drawn inspiration from spiral blades and undertaken comprehensive enhancements and optimization designs in order to fulfil the specifications pertaining to the diameter and depth of deep pits.

Jiang, *(1997)*, conducted a study to determine the critical speed of soil lifting motion for spiral blades. This investigation involved analysing the movement and stress experienced by individual soil units on the spiral surface of the drill bit. The aim was to investigate the relationship between the parameters of the spiral surface and the critical speed required for effective soil lifting. In accordance with this theoretical framework, scientists have developed a range of pond excavation apparatuses in order to meet the specific criteria pertaining to hole dimensions and functional objectives.

Liu et al., (2018), conducted an analysis of the operational mechanism of a portable hole forming machine and afterwards derived the structural parameters of the hole forming device based on the desired hole size. The effectiveness of the device's operation was then validated by field trials. A portable device has been developed for the purpose of facilitating tobacco transplantation in mountainous regions, specifically designed to create pond mouths. During the computation of structural characteristics, the soil is simplified as an isotropic elastic-plastic material, and the necessary aperture size is generated by means of a drilling tool *(Yu et al., 2018)*. The aforementioned studies address the issue of pre-transplanting digging in the context of tobacco cultivation. However, upon the completion of the digging device operation, mechanized transplanting becomes challenging due to problems such as ground wheel slip and unstable tractor forward speed. These issues hinder the ability of the transplanting machine to effectively plant seedlings into the pre-dug pits. Consequently, the process of manual transplantation is typically conducted subsequent to the mechanical excavation procedure.

The aforementioned issues serve as adequate examples to demonstrate the pressing need for resolving the integrated process of pit digging and transplanting in tobacco cultivation. Numerous academic investigations have been undertaken by scholars in relation to this subject matter. The duckbill transplanting mechanism is widely employed in dryland transplanting machines, making it the prevailing choice in this context. By manipulating the horizontal movement and speed of the duckbill mechanism, the machine can effectively control the forward speed and assure the proper alignment of the seedling during the direct planting process into the soil.

Xiong et al., (2020), designed the structural parameters of the duckbill planter based on the hole size, and optimized the motion trajectory through simulation, enabling the duckbill planter to squeeze out a hole in the soil while transplanting.

Fan et al., (2019), designed a self-propelled tobacco transplanting machine that uses a parallel four bar mechanism to control the duckbill planter for transplanting operations, forming a hole in the soil while transplanting. Despite the above researches demonstrated feasibility in hole digging and transplanting, it is crucial to acknowledge a notable limitation: the resulting holes are both small and irregular, posing challenges in meeting the agricultural demands for deep hole planting of tobacco seedlings.

In response to the above problems, this study combined the specific requirements of hole size and transplanting uprightness to design a multifunctional tobacco transplanter that integrates a digging mechanism and a transplanting mechanism, which realizes digging and transplanting simultaneously.

MATERIALS AND METHODS

Agronomic requirements

The tobacco seedlings were transplanted beneath a mulch film utilizing robust seedlings that were 35-40 days old and measured 5-8 cm in height *(Yao, 2017; Lu, 2015)*. As depicted in Figure 1, it is important to excavate pits prior to planting in order to provide an appropriate living environment for tobacco seedlings subsequent to transplantation. The deep pit has a top diameter ranging from 30 to 35 cm, a depth ranging from 15 to 20 cm, and a plant spacing of 55 to 65 cm.

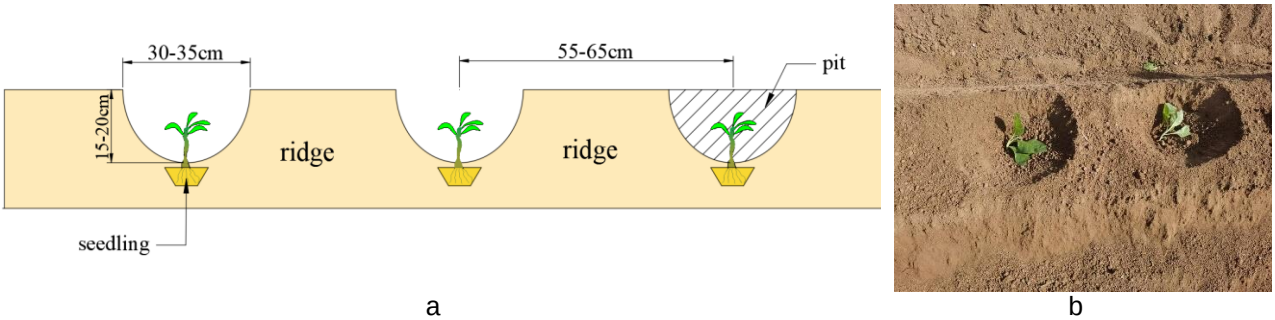

a b

Fig. 1- Agronomy of tobacco seedling transplantation under film

Overall structure and working principle

A tobacco transplanting device based on a parallel four bar mechanism was designed to meet the requirements of agronomy while also achieving the integration of excavation and transplanting processes. The device consists of rotary tillage device, seedling feeding device, pond digging device, transplanting device, and transmission system. The ground wheel powers the movement of the seedling feeding device and the four bar mechanism device. Figure 2 depicts the overall structure.

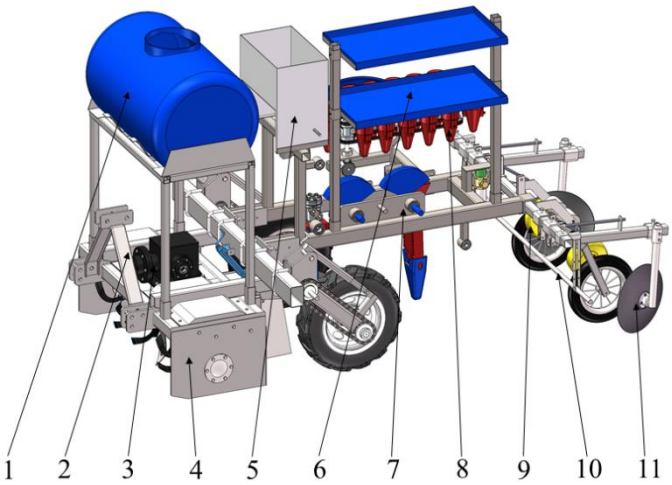

Fig.2-Structure diagram of the entire machine.

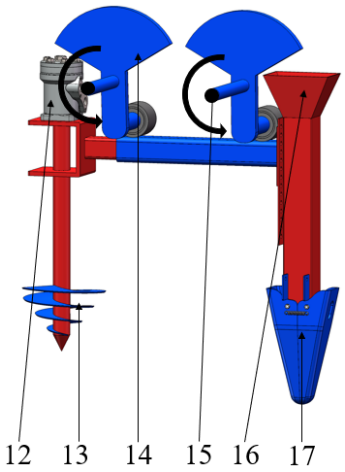

Fig.3-Structural diagram of the integrated mechanism for digging and transplanting.

1. Water tank; 2. Three point suspension device; 3. Reduction gearbox; 4. Rotary tillage device; 5. Fertilizer box; 6. Loading seedling trays; 7. Four bar mechanism; 8. Seedling feeding device; 9. Film pressing wheel; 10. Film covering device; 11. Earth cover wheel; 12. Hydraulic motor; 13. Spiral blades; 14. Counterweight block; 15. Rotation centre; 16. Falling seedling mouth; 17. Duckbill planter.

During the operational phase, the operator transfers the seedlings from the seedling tray and inserts them into the suspended cup of the seedling division device. The seedling division device and the four bar mechanism device exhibit simultaneous movement. When the seedling receiving aperture of the duck beak planter ascends to its highest position, the suspended cup initiates its opening mechanism, causing the tobacco seedlings to descend into the duck beak, so accomplishing the operation of seedling deployment. The completion of the works of digging and transplanting is facilitated by a device that combines a parallel four bar mechanism and is controlled by a transmission system. The duckbill planter is utilized to relocate tobacco seedlings to the precise location within the hole created by the digging mechanism.

Integrated operation device for digging and transplantation structural design

A digging transplanting mechanism has been devised, which utilizes a parallel four-bar mechanism to achieve integrated operation of digging and transplanting. The working principle and motion trajectory are depicted in Fig. 4. Two cranks exhibit a counterclockwise rotational motion around a shared centre of rotation, with both cranks rotating at an equivalent speed. Simultaneously with the rotation of the crank, the hydraulic motor propels the spiral blades of the excavation apparatus, causing them to rotate and create perforations on the ridge. The motion trajectory of the device is determined by four parameters, namely the length of the connecting rod, the forward speed of the implement, the speed of the crank, and the length of the crank. This can be observed from the working principle.

Parameters λ are typically provided to describe the composite motion that consists of both rotation and translation in the integrated process of excavation and transplantation.

In order to streamline the computation process, as demonstrated in equation (1), Fig 5 describes the law of influence on trajectory of the parameters λ.

$$\lambda = \frac{l\omega}{v} \tag{1}$$

Note: l is the length of the crank, (mm); ω is the crank speed, (rpm); v is the forward speed of the implement (m/min).

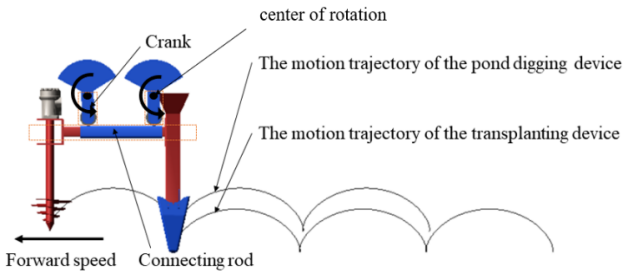

Fig. 4 - Motion trajectory diagram of the integrated mechanism for digging and transplanting

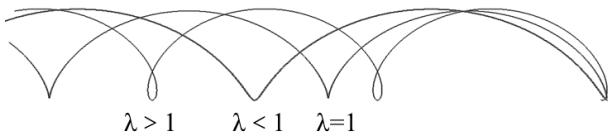

Fig. 5 - The law of influence on trajectory of the parameters λ

To ensure the vertical alignment of seedlings upon transplantation, it is imperative to maintain a value of λ equal to 1. The interdependence between the velocity of the implement and the speed at which planting occurs can be elucidated through the utilization of Formula 2, given that the implement is propelled by ground wheels.

$$\frac{v}{p} = d \tag{2}$$

Note: v is the forward speed of the implement, (m/min); p is the transplanting rate, (plants/min); d is the plant spacing, (m).

When determining the parameters for the connecting rod design, the distance between plants is selected as the intermediate value of 0.5 m. This implies that the length of the connecting rod is 0.5 m. According to the "*Operation Standards for Dryland Transplanters"*, it is stipulated that the operational efficiency of dryland transplanting machines must be equal to or greater than 35 plants per minute, although the upper limit of efficiency should normally not surpass 55 plants per minute. Hence, by supposing a constant rate of 45 plants per minute, the velocity of the machines may be determined as v=27 m/min. When the planting rate is 45 plants per minute, the angular velocity (ω) is equal to crank speed. By substituting the numerical value into equation (1), the resulting crank length is determined to be l=9.6 cm.

Designing parameters for spiral blades

During the excavation process, the soil is propelled upwards by the rotational movement of spiral blades, resulting in the formation of pits. Hence, throughout the soil displacement process, the motion of the soil can be categorized into two distinct phases. The initial phase involves the vertical displacement of the soil, wherein the dirt ascends in conjunction with the rotational motion of spiral leaves, so creating the essential depressions for the cultivation of tobacco seedlings. The subsequent phase involves the parabolic trajectory of the soil.

Factor analysis of soil lifting movement

The movement and stress of the soil at the interface between the outer edge of the spiral blade and the pit wall were investigated by researchers *(Xiao, 2010)*. The deduction made by the researcher states that when the relative velocity of the soil unit is zero (V_r=0), and the angle between the absolute velocity and the horizontal plane is zero (β=0), the critical speed formula for the rotation of the spiral blade, which allows the soil to rise, is as follows:

$$n_k = 9.6\sqrt{\frac{g\tan(\alpha+\varphi_1)}{(1-\frac{\tan\zeta}{\tan\alpha})^2 r_0 f_2}} \tag{3}$$

Note: g - Aacceleration of gravity; α- The spiral angle at the outer edge of the spiral surface, (°); φ_1- Friction angle between soil and spiral surface, (°); ξ- The angle between the velocity of soil particles at the outer edge of the spiral surface and the horizontal plane, (°); r_0- Drill radius, (mm); f_2- The internal friction coefficient of the soil, (N).

The relationship between the spiral angle and radius of the spiral blade and the critical speed of soil lifting motion can be observed from equation (3). Hence, it is imperative to ascertain the appropriate range of two variables in order to establish a factual foundation for subsequent simulation and optimization studies.

The range of outer diameter and helix angle for spiral blades

Figure 6 displays the three-dimensional representation of the spiral blade.

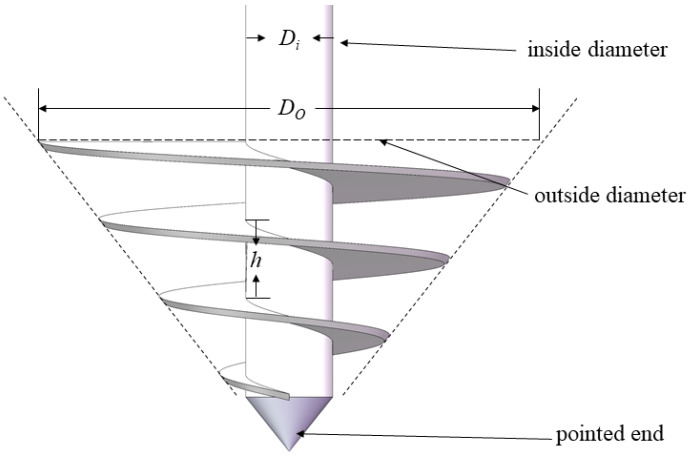

Fig. 6 - Three-dimensional view of spiral blades

h – Pitch, (mm); D_i- Diameter of central axis, (mm); D_O- Maximum diameter of spiral blade, (mm).

The diameter range of the pond mouth is determined by agricultural criteria, namely falling within the range of 350 mm to 400 mm. Additionally, the outer diameter D_0 of the drill bit must satisfy formula (4) *(Ba, 2022)*. Hence, the range of D_0 is determined to be 322 mm to 392 mm.

$$0.92D \le D_O \le 0.98D \tag{4}$$

Once the range of the outer diameter of the spiral blade has been established, the remaining structural parameter that needs to be determined is the spiral lift angle. The mathematical expression used to determine the spiral rising angle is as follows:

$$\gamma = \arctan\frac{h}{\pi D_i} \tag{5}$$

Note: γ is the spiral rising angle, (°).

The investigation conducted by researchers on the spiral rise angle has revealed that the design parameters for spiral rise angle must adhere to the constraints outlined in formula (6) *(Lu et al., 2022; Yang et al., 2020; Giuseppe et al., 2021)*.

$$\gamma \le 90^o - (\rho_1 + \rho_2) \tag{6}$$

Note: ρ_1 is the friction angle between soil and steel, (°); ρ_2 is the friction angle between the soil, (°).

Upon reviewing the related data, it was determined that the value of ρ_1 is 30°, whereas the value of ρ_2 is 40° *(Qin et al., 2016; Gao et al., 2015)*. Based on the given information, it can be inferred that the value of α is less than or equal to 20 degrees. Currently, the spiral rise angle of the excavated spiral blades is all above 15 °. Therefore, the range of spiral rise angles considered is limited to values between 15° and 20°.

The range of spiral blade speeds

Based on equation (3), it can be deduced that in the absence of contact between the spiral blade and the soil (ξ=0), the critical speed of the spiral blade is denoted as $n_k = 9.6g\tan(\alpha + \varphi_1)/r_0 f_2$.

However, it should be noted that the critical speed under these conditions does not hold any practical significance. The purpose of spiral blade rotation lies in generating upward motion force for soil displacement. Therefore, it is imperative to do kinematic and mechanical analyses on the soil unit within the context of soil flow. These analyses aid in determining the appropriate range of rotational speeds for the spiral blades.

Figure 7 depicts the force study conducted on the particles comprising the soil flow unit.

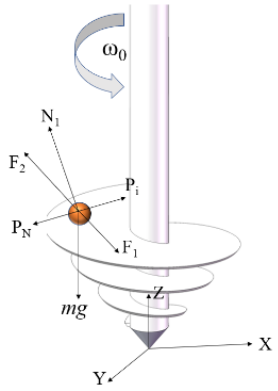

Fig. 7 - Force analysis of soil particle units

When the spiral blades undergo a consistent rotational velocity, the soil unit situated on these blades experiences many distinct forces. These forces consist of the gravitational force, denoted as mg, exerted on the soil unit due to gravity, as well as the positive pressure, labelled as f_1, exerted by the inner soil on the soil unit. Furthermore, there are other forces that are being exerted.

The supporting force (N_1) of spiral blades on soil units.

$$N_1 = mg\cos\gamma \tag{7}$$

The frictional force (F_1) of spiral blades on soil units.

$$F_1 = f_1 N_1 \tag{8}$$

The inertial centrifugal force (P_N) of the soil unit.

$$P_N = mr\omega_0^2 \tag{9}$$

Note: In the formula, r is the distance between the soil unit and the axis of rotation, (mm).

The positive pressure (P_i) of the outer soil on the soil unit.

$$P_i = P_N \tag{10}$$

The frictional force F_2 of the outer soil on the soil unit.

$$F_2 = f_2 P_i \tag{11}$$

After determining the force on soil particles, by calculating the acceleration and centrifugal force of the soil unit, one can directly assess the soil particles' motion status. The absolute acceleration of the soil unit can be determined as it is situated on the spiral surface of a uniformly rotating drill bit and moves in an upward direction with respect to the spiral surface.

$$a_a = a_e + a_r + a_k \tag{12}$$

Note: In the formula, a_e - implicated acceleration; a_r - relative acceleration; a_k Coriolis acceleration.

$$a_e = a_{en} + a_{e\tau} \tag{13}$$

$$a_r = a_{rn} + a_{r\tau} \tag{14}$$

$$a_{e\tau} = a_{r\tau} = 0 \tag{15}$$

Note: In the formula, a_{en} is the normal acceleration of the implicated motion; $a_{e\tau}$ is the tangential acceleration of the motion involved; a_{rn} is the normal acceleration of relative motion; $a_{r\tau}$ is the tangential acceleration of relative motion.

$$a_{en} = r\omega_0^2 \tag{16}$$

$$a_{rn} = \frac{v_r^2}{\rho} \tag{17}$$

Note: In the equation, ω_0 is the normal rotational speed, (rpm); v_r is the velocity of movement at the soil unit (mm/s); ρ is the curvature radius of the helix at the soil unit.

$$\rho = \frac{r}{\cos^2\gamma} \tag{18}$$

$$a_k = 2\omega_0 v_r \sin(90^o + \gamma) = 2\omega_0 v_r \cos\gamma \tag{19}$$

On the basis of equations (12) to (19), the absolute acceleration of the soil unit is calculated as follows:

$$a_a = r\omega_0^2 + \frac{v_r^2 \cos^2 \gamma}{r} - 2\omega_0 v_r \cos\gamma \tag{20}$$

Because of $v_r \cos\gamma$, it is the projection of v_r on the horizontal plane v_{rx}, so the absolute acceleration of the soil unit is:

$$a_a = r\left(\omega_0 - \frac{v_{rx}}{r}\right)^2 \tag{21}$$

From this, it can be determined that the soil unit's centrifugal force F_c is:

$$F_c = mr\left(\omega_0 - \frac{v_{rx}}{r}\right)^2 \tag{22}$$

The following equation is obtained by projecting the forces operating on the soil unit onto the X, Y, and Z axes:

$$f_2 P_i - f_2 F_3 - f_1 N_1 - mg\sin\gamma = 0 \tag{23}$$

$$N_1 - mg\cos\gamma = 0 \tag{24}$$

$$P_i - F_3 - P_N = 0 \tag{25}$$

Combining formulations (23) through (25) leads to the conclusion that:

$$mr\left(\omega_0 - \frac{v_{rx}}{r}\right)^2 = \frac{mg\left(f_1\cos\gamma + \sin\gamma\right)}{f_2} \tag{26}$$

The critical speed of the spiral blade is achieved when the soil unit remains stationary in relation to the blade's rotation. Hence, as equation (26), the critical angular velocity of the spiral blade can be determined.

$$\omega_0 = \sqrt{\frac{g\left(f_1\cos\gamma + \sin\gamma\right)}{rf_2}} \tag{27}$$

The critical speed of the spiral blade is:

$$n_0 = \frac{30}{\pi}\omega_0 = 9.6\sqrt{\frac{g\left(f_1\cos\gamma + \sin\gamma\right)}{rf_2}} \tag{28}$$

Note: In the formula, f_1 is the friction coefficient between the soil and the spiral surface, and f_2 is the friction coefficient between soil particles.

By integrating the data on spiral blade diameter and spiral angle, it can be determined that the critical speed falls between the range of 138.36 rpm to 188.22 rpm. To ensure the proper upward movement of the soil, the simulation test requires a minimum speed that is determined by calculating the highest critical value theoretically. This value is found to be 188.22 rpm.

In the drilling procedure, it is imperative to implement measures that prevent the soil ejected during drilling from infiltrating the pre-existing well, as depicted in Fig 8. The distance at which soil is ejected is directly influenced by the centrifugal force imposed on soil particles by the spiral blades. Therefore, the optimal rotational speed of the spiral should be determined by the rotational speed at which the soil particles no longer fall into the prepared pit.

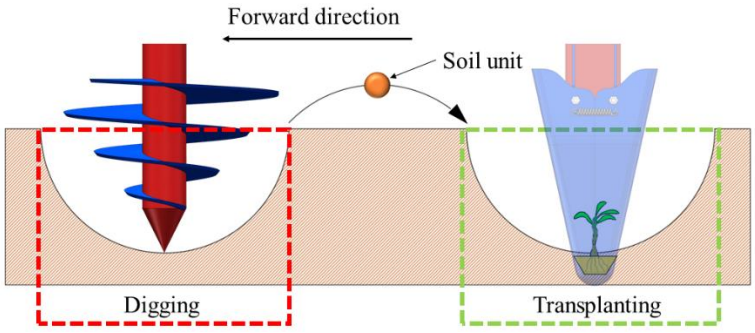

Fig. 8 - Schematic diagram of soil flowing into other pits

When doing theoretical calculations, it is imperative to take into account the minimum distance at which soil can infiltrate a previously excavated pit. By integrating the design parameters of pit size and plant spacing, a minimum distance of 250 mm can be determined. According to the data presented in Figure 9, the forces experienced during soil ejection encompass the influence of gravity as well as the forces exerted by spiral blades. Consequently, the trajectory of soil particles during ejection can be regarded as a form of oblique projectile motion. By utilizing equation (22), it is determined that the distance covered during soil ploughing is 250 mm when the rotational speed is 373.7 rpm.

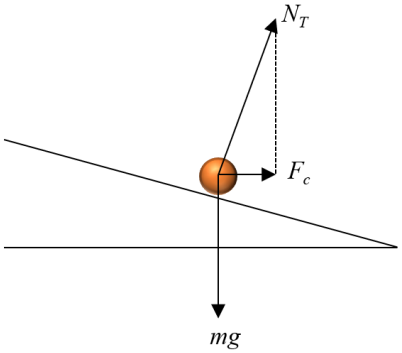

Fig. 9 - Force analysis of soil particles at the moment of being thrown out

N_T represents the force exerted by the spiral blade on soil particles at the moment when the soil is thrown out

Discrete element simulation optimization

Based on the aforementioned theoretical study, it has been ascertained that the primary factors influencing the dimensions of the pit are the spiral angle z_1 (x_1), the outer diameter z_2 (x_2) of the spiral blade, and the rotating speed z_3 (x_3) of the spiral blade. The experiment involves two indicators, specifically the depth of the hole (y_1, measured in millimetres) and the diameter (y_2, also measured in millimetres). Table 1 displays the experimental factors and corresponding levels.

Table 1. Experimental factors and levels

Factors / Levels	Spiral rising angle z_1 (°)	Spiral blade outer diameter z_2 (mm)	Spiral blade speed z_3 (rpm)
1	15	322	188.22
2	17.5	357	280.96
3	20	392	373.70

The present study utilizes a three factors binary regression orthogonal combination design and incorporates three zero point tests (m_0=3), resulting in an obtained r^2=1.831 *(Li et al., 2005; Li et al., 2005)*. Prior to conducting the experiment, it is imperative to encode the natural elements *(Zhuang et al., 1992; Zheng, 2004; He, 2013)*, as illustrated in Table 2.

Table 2. Test factor coding table

$x_j(z_j)$	z_1	z_2	z_3
$r(z_{2j})$	20	392	373.70
$1(z_{0j}+\Delta_j)$	19.3477	382.8684	349.504
$0(z_{0j})$	17.5	357	280.96
$-1(z_{0j}-\Delta_j)$	15.6523	331.1316	212.416
$-r(z_{1j})$	15	322	188.22
$\Delta_j=(z_{2j}-z_{1j}).(2r)^{-1}$	1.8477	25.8684	68.5440
$x_j=(z_j-z_{0j}).(\Delta_j)^{-1}$	$0.5412(z_1-17.5)$	$0.0387(z_2-357)$	$0.0146(z_3-280.96)$

Numerous academics have undertaken research on the intrinsic and contact properties of soil and steel in the extant body of literature. Hence, by the examination of relevant literature, the parameters utilized in the discrete element simulation are identified and shown in Table 3 *(Song et al., 2022; Tekeste et al., 2018; Sun et al., 2022)*.

Table 3. Basic simulation parameter settings

Parameter			Value
Intrinsic parameter	Soil	Density/(kg.m^{-3})	2679
		Shear modulus/(Pa)	1.2e+5
		Poisson's ratio	0.36

Parameter			Value
	Spiral blade	Density/(kg.m^{-3})	7810
		Shear modulus/(Pa)	2.07e+11
		Poisson's ratio	0.3
Contact parameter	Soil-soil	Restitution coefficient	0.2
		Static friction coefficient	0.4
		Rolling friction coefficient	0.3
	Soil- spiral blade	Restitution coefficient	0.5
		Static friction coefficient	0.5
		Rolling friction coefficient	0.3

The simulation process is represented in Fig. 10, and the pits following the simulation operation are displayed in Fig. 11.

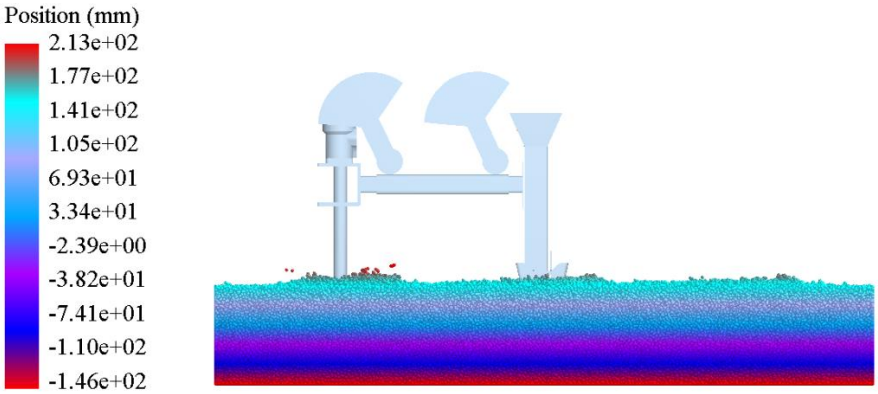

Fig. 10 - Simulation test process

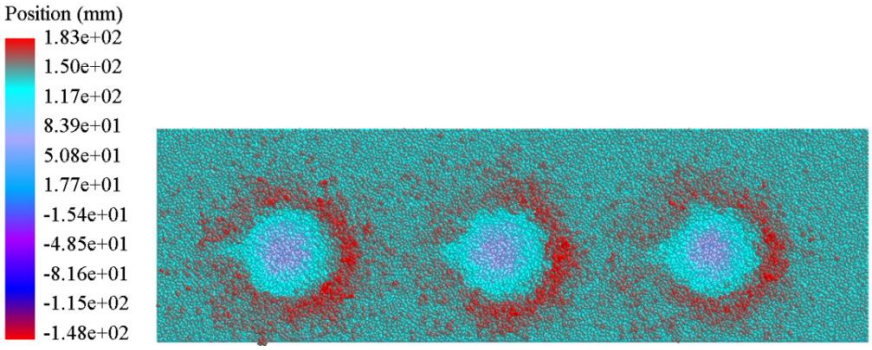

Fig. 11 - Simulation test effect

RESULTS AND DISCUSSION

Test results

The test results are presented in Table 4.

Table 4. Design of experiments results

Test	x_1	x_2	x_3	x_1x_2	x_1x_3	x_2x_3	x_1^2	x_2^2	x_3^2	y_1	y_2
1	-1	-1	-1	1	1	1	1	1	1	135	260
2	1	-1	-1	-1	-1	1	1	1	1	170	308
3	-1	1	-1	-1	1	-1	1	1	1	169	310
4	1	1	-1	1	-1	-1	1	1	1	188	342
5	-1	-1	1	1	-1	-1	1	1	1	162	306
6	1	-1	1	-1	1	-1	1	1	1	187	345
7	-1	1	1	-1	-1	1	1	1	1	181	343
8	1	1	1	1	1	1	1	1	1	198	380
9	$-r$	0	0	0	0	0	r^2	0	0	140	286
10	r	0	0	0	0	0	r^2	0	0	187	349
11	0	$-r$	0	0	0	0	0	r^2	0	164	287
12	0	r	0	0	0	0	0	r^2	0	194	348
13	0	0	$-r$	0	0	0	0	0	r^2	158	285
14	0	0	r	0	0	0	0	0	r^2	189	349
15	0	0	0	0	0	0	0	0	0	180	328
16	0	0	0	0	0	0	0	0	0	180	328
17	0	0	0	0	0	0	0	0	0	180	328

The depth and diameter of pits were acquired by a three factors binary regression orthogonal combination experiment, conducted under various parameter combinations. Fig.12 illustrates the juxtaposition of the test value curves and fit value curves of two regression models. The blue line corresponds to the measured value of the test, whereas the red line shows the value obtained from fitting the sample. It is evident that these two groups of numbers exhibit a high degree of proximity.

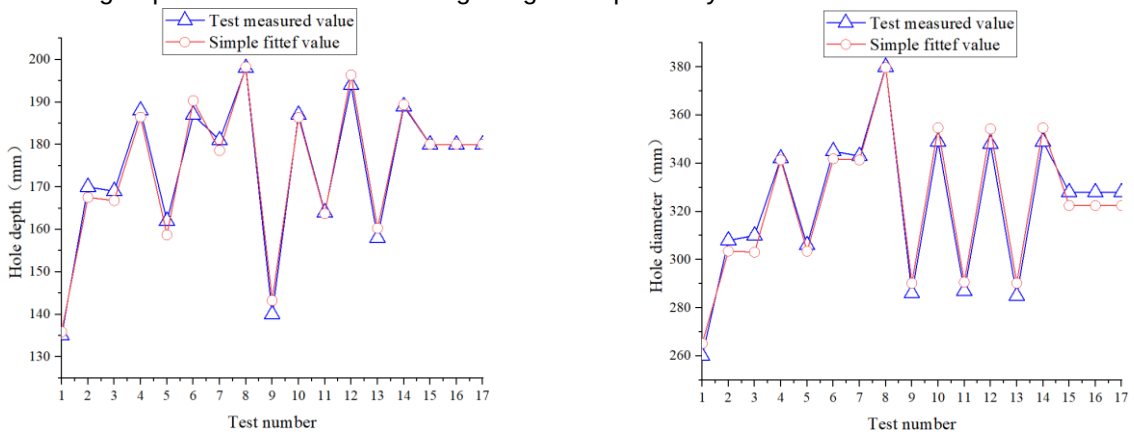

Fig. 12 - Comparison of measured and fitted values

According to the findings presented in Table 5, the P-values for both models are below the threshold of 0.01. This suggests that the models exhibit a high level of statistical significance, suggesting their ability to effectively predict the values of pit depth and pit diameter. The determination coefficients R^2 for the two models are 0.9659 and 0.9740, respectively. These values suggest that the regression models are able to account for 96.59% and 97.4% of the observed cases, respectively. The coefficient of variation (C.V.) for the two data sets is 1.48% and 1.65%, respectively. The aforementioned pair of primary values signifies a substantial level of concordance between the projected values of the regression equation and the observed measured values.

After removing insignificant factors, the binary regression equation for pore depth and pore diameter is obtained as follows:

$$y_1 = -1820.9436 + 128.45z_1 + 2.84z_2 + 1.3531z_3 - 0.097z_1z_2 - 0.0024z_2z_3 - 2.4345z_1^2 - 0.0006z_3^2 \quad (30)$$

$$y_2 = -325.7619 + 12.9034z_1 + 0.9098z_2 + 0.3474z_3 \quad (31)$$

Based on equation (30), there exists a positive linear relationship between the depth of the hole (y_1) and the spiral angle (x_1), the outer diameter of the spiral blade (x_2), and the rotational speed of the spiral blade (x_3). Based on equation (31), there exists a positive linear relationship between the hole diameter y_2 and the spiral angle x_1, the outer diameter x_2 of the spiral blade, and the rotational speed x_3 of the spiral blade. This phenomenon can be attributed to the three components theory, wherein it is seen that a greater spiral angle has the potential to enhance the soil's fluidity, hence facilitating its expulsion from the hole. There is a positive correlation between the outer diameter of the spiral blade and the diameter of the drilled hole. The depth of a hole is determined by the angle of repose of soil particles when the hole diameter is bigger. The upward lifting force exerted by the spiral blade is directly proportional to the rotational speed of the spiral blades. Hence, an increase in rotating speed results in an augmented vertical and horizontal displacement of the soil, as well as a deeper excavation. This finding aligns with the research outcomes of Meng and Gao *(Gao. 2018; Meng. 2007)*.

Table 5. Analysis of hole related data

Source	Hole depth				Hole diameter			
	Sum of Squares	Mean Square	*F* Value	*P*-Value	Sum of Squares	Mean Square	*F* Value	*P*-Value
Model	5063.27	562.59	86.00	< 0.01**	15087.08	1676.34	54.54	< 0.01**
x_1	2243.60	2243.60	342.96	< 0.01**	5024.54	5024.54	163.47	< 0.01**
x_2	1284.63	1284.63	196.37	< 0.01**	4896.33	4896.33	159.30	< 0.01**
x_3	1021.91	1021.91	156.21	< 0.01**	5012.34	5012.34	163.07	< 0.01**
x_1x_2	72.00	72.00	11.01	0.0128*	40.50	40.50	1.32	0.2887
x_1x_3	18.00	18.00	2.75	0.1411	2.00	2.00	0.0651	0.8060
x_2x_3	60.50	60.50	9.25	0.0188*	18.00	18.00	0.5856	0.4691
x_1^2	321.15	321.15	49.09	< 0.01**	46.60	46.60	1.52	0.2580
x_2^2	0.2295	0.2295	0.0351	0.8567	46.60	46.60	1.52	0.2580
x_3^2	36.60	36.60	5.59	0.0499	55.06	55.06	1.79	0.2226
Residual	45.79	6.54			215.15	30.74		
Lack of Fit	45.79	9.16			215.15	43.03		
Pure Error	0	0			0	0		
	R^2=0.9659; C.V.=1.48%				R^2=9740; C.V.=1.65%			

*Note: 0.01 < p < 0.05 (significant, *); 0.001 < p < 0.01 (highly significant, **).*

Table 5 demonstrates the significant influence of various factors on the depth of the hole. Firstly, the spiral angle (x_1) exhibits a highly significant impact on the depth of the hole (y_1) (P<0.01). Secondly, the outer diameter of the spiral blade (x_2) also displays an extremely significant influence on y_1 (P<0.01). Additionally, the helical blade speed (x_3) significantly affects the depth of the hole (y_1) (P<0.01). Furthermore, the interaction term x_1x_2, representing the combined effect of the spiral rising angle and the outer diameter of the spiral blade, significantly impacts y_1 (P<0.05). Similarly, the interaction term x_2x_3, representing the combined effect of the outer diameter of the spiral blade and the drilling speed of the spiral blade, significantly influences the depth of the hole (y_1) (P<0.05). Moreover, the square term x_1^2, representing the squared value of the spiral rise angle, significantly affects y_1 (P<0.01). However, it is worth noting that the remaining experimental factors do not exhibit a significant impact on the depth of the hole (y_1). Upon disregarding the negligible factors, the examination of the F-value reveals that the relative impact of each significant factor on the depth of pores follows the sequence $x_1>x_2>x_3>x_1^2>x_1x_2>x_2x_3$. This observation aligns with the functioning of the spiral blades of the excavator as investigated by Guo *(Guo et al., 2003)*. The spiral angle (x_1) exhibits a statistically significant effect on the pore diameter (y_2) with a p-value less than 0.01. Similarly, the outer diameter (x_2) of the spiral blade demonstrates an extremely significant influence on the hole diameter (y_2) with a p-value less than 0.01. Additionally, the helical blade speed (x_3) also exhibits an extremely significant impact on the hole diameter (y_2) with a p-value less than 0.01. Upon disregarding the negligible components, it becomes evident through a comparison of the F value that the three primary terms exhibit a very similar influence on the pore diameter. This finding aligns with the research outcomes of scholars investigating the interplay between conical spiral drills and soil *(Jin, 2022)*.

Response surface analysis

Based on the analysis of the response surface depicted in Fig 13, it is evident that the hole depth exhibits a positive correlation with the spiral angle x_1 when the drilling speed of the spiral blade is 280.96 rpm. Furthermore, the rise of this correlation follows a non-linear pattern, characterized by an initial increase, followed by a subsequent decrease. There is a positive correlation between the increase in diameter x2 of the spiral blade and the rising trend observed in the depth of the hole. When the spiral angle (x_1) is equal to 20 degrees and the outside diameter of the spiral blade (x_2) measures 392 mm, the depth of the hole (y_1) is determined to be 187 mm. The hole depth (y_1) exhibits a positive correlation with the spiral angle (x_1) as the outside diameter (x_2) of the spiral blade increases to 357 mm. There is a positive correlation between the increase in the outer diameter (x_2) of the spiral blade and the corresponding rise in the hole depth (y_1). When the helix angle (x_1) is equal to 17.5 degrees, the depth of the hole (y_1) measures 192 mm. There is a positive correlation between the increase in the outer diameter (x_2) of the spiral blade and the corresponding rise in the hole depth (y_1). An rising trend in hole depth (y_1) is observed when the rotational speed (x_3) of the spiral blade increases. When the outside diameter (x_2) of the spiral blade measures 392 mm and the rotating speed (x_3) of the spiral blade is 373.7 rpm, the depth (y_1) of the hole is 186 mm. The contour plot reveals the presence of a non-linear relationship between the spiral angle (x_1) and the outer diameter (x_2) of the spiral blade. This suggests a notable interaction between these two variables. When the helix angle (x_1) is 20° and the helix blade speed (x_3) is 373.7 rpm, the depth of the hole (y_1) is 183 mm. A discernible circular arc can be shown between the spiral rising angle (x_1) and the spiral blade speed (x_3), suggesting that the interaction between these two variables is not substantial. A notable interaction is observed between the outer diameter (x_2) of the spiral blade and its rotating speed (x_3), as evidenced by the presence of a non-parallel line segment.

Lead angle(x_1) and
Spiral blade outer diameter (x_2)
(x_3=280.96 rpm)

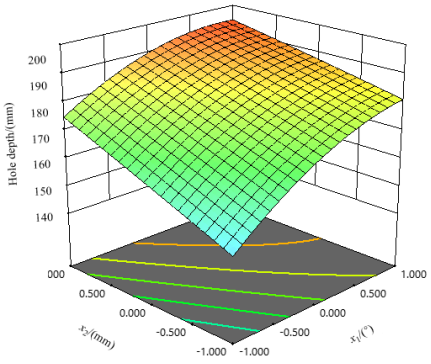

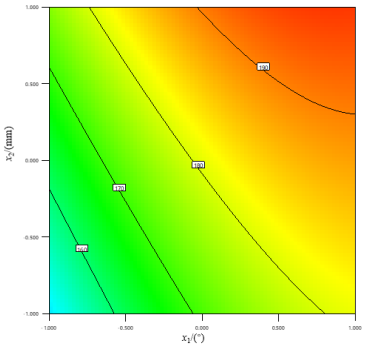

Lead angle(x_1) and Spiral blade speed (x_3) (x_2=357 mm)

Spiral blade outer diameter (x_2) and Spiral blade speed (x_3) (x_1=17.5°)

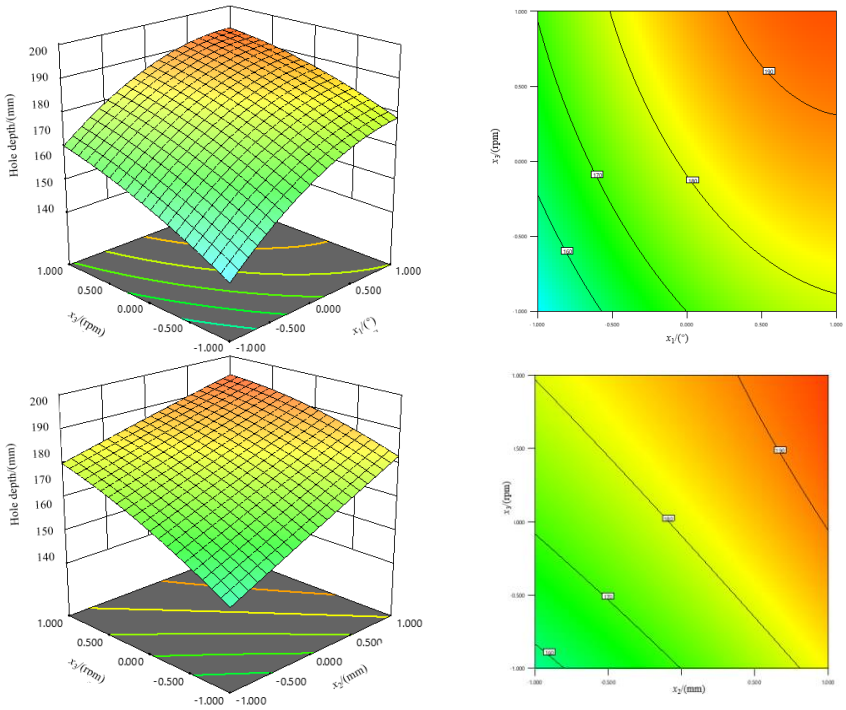

Fig. 13 - 3D response surface and 2D contour maps of hole depth

Parameter optimization

The regression equations for the two indicators are accompanied by a description of their maximum and lowest values, as presented in Table 6. The data presented in Table 8 reveals that the depths of the holes are consistently below 200 mm. The regression equation yields a minimum pore diameter value of 303.575 mm and a maximum pore diameter value of 374.26 mm, as indicated by the data.

Table 6 Maximum and minimum values in the regression equation

Test indicators			Test Factors		
			z_1	z_2	z_3
Hole depth	max	197.036	18.658	377.811	225.812
	min	134.443	16.013	336.189	197.036
Hole diameter	max	374.260	18.987	377.811	336.104
	min	303.575	18.987	336.189	225.816

During the pre-transplantation excavation process, it is imperative to create a hole of maximum size within the agronomic parameters to guarantee ample development space for tobacco seedlings. Hence, the optimization objectives were determined to be a hole depth of 200 mm and a hole diameter of 350 mm. According to the data presented in Table 6, the hole maximum depth measures 197.036 mm. Consequently, the optimization objective for the simulation experiment was determined to be the maximum value of the hole regression equation. The optimization target for the hole diameter is chosen to be 350 mm, and the relevant values for the factors are presented in Table 7.

Table 7. Optimization objectives

Optimization objectives and values		Test Factors		
		z_1	z_2	z_3
Hole depth (mm)	197.036	18.658	377.811	197.036
Hole diameter (mm)	350	18.987	375.158	257.818

Table 7 provides an overview of the range of intervals that have been optimized for three parameters. However, it is necessary to further optimize these three intervals by determining three specific values. The regression equation reveals that the coefficients associated with the three main terms are all positive, indicating a positive relationship between the value of the regression equation and the growth in the three components. Hence, the approach involves identifying the highest value within the specified range of factors and utilizing an integer as the precise value for the purpose of optimization, as depicted in Table 8. Based on the integration of the regression equation, it can be inferred that the optimal hole depth is 193 mm, while the hole diameter measures 350 mm.

Table 8. Specific values after optimization

Test Factors			Test indicators	
z_1(°)	z_2(mm)	z_3(mm)	Hole depth (mm)	Hole diameter (mm)
19	378	258	193	350

Field validation test

In order to validate the outcomes of simulation optimization, a prototype was manufactured based on the parameters that were optimized through simulation trials. Subsequently, field experiments were carried out to assess the performance of the prototype.

The location of the experimental site is situated in Honghe Prefecture, in Yunnan Province, China. The soil composition at this site is characterized as sandy loam. The test site is depicted in Figure 14. Choose seedlings that have the age of 38 days and have favourable growth characteristics, namely seedling heights that fall within the range of 50 mm to 80 mm. Prior to conducting the experiment, a rotary tiller is employed in order to thoroughly pulverize the soil. Following the transplantation of 300 seedlings, it is imperative to gather pertinent data pertaining to the hole.

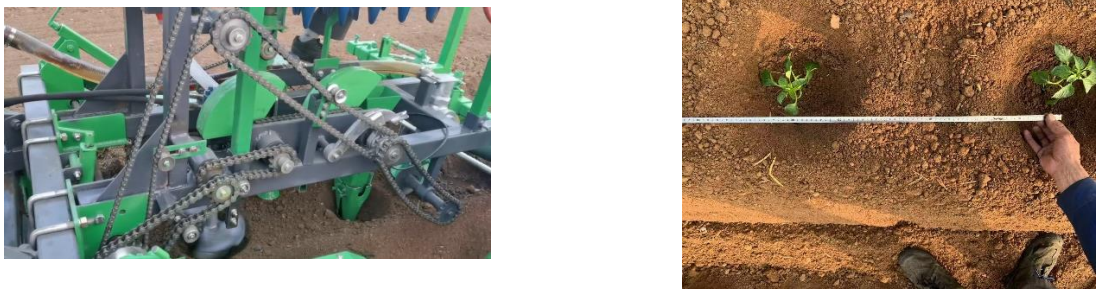

a. Test site **b. After transplanting**

Fig. 14 - Field experiment

The primary data acquired include measurements of hole depth and hole diameter. The mean depth and diameter of holes obtained from field testing were 191 mm and 347 mm, respectively. The numerical value closely approximates the outcome of the simulated optimization.

CONCLUSIONS

(1) The present study developed a tobacco planting device utilizing a parallel four-bar mechanism, which combines the advantageous characteristics of a spiral blade for hole excavation and a duckbill transplanting device for substrate seedling transplantation. To achieve simultaneous execution of excavation and transplanting procedures, the crank length is established as 9.6 cm, while the connecting rod length is set to be 50 cm. These measurements are calculated through the utilization of trajectory technology and theoretical calculations, taking into account the spatial separation between plants. This apparatus integrates the processes of excavation and transplantation to achieve the mechanical operation of tobacco planting.

(2) The present study involved an examination of the relationship between the spiral blades and the soil, with a focus on identifying the primary factors influencing the formation of holes. These factors encompassed the spiral lift angle, the maximum outer diameter of the spiral blades, and the rotational speed at which the blades operated. The calculation of the range of the three parameters was conducted in order to satisfy the agronomic prerequisites for tobacco cultivation. The values provided encompass a range of measurements: 15-20° for angles, 322-392 mm for lengths, and 188.22-373.30 rpm for rotational speeds.

(3) A simulation test was conducted using the discrete element method to investigate the effects of a three factors three-level regression orthogonal design. The test factors were optimized for the experiment. The findings of the optimization analysis indicate that a spiral lift angle of 19°, a maximum spiral blade diameter of 378 mm, and a rotational speed of 258 rpm result in the desired outcome for the pit. The depth of the hole is 193 mm, while its diameter measures 350 mm.

REFERENCES

[1] Ba, L. Z. (2022). *Design and experiment of orchard fertilizer digging machine*. Shanxi Agricultural University; DOI: 10.27285/d.cnki.gsxnu.2022.000647.

[2] Chen, X., Shi, L., Yuan, K., Wang, K. P. (2014). Discussion on the technology of flue-cured tobacco seeding transplant under plastic film. *Journal of Agriculture Sciences*, 1963-1964+1972. DOI: 10.13989/j.cnki.0517-6611.2014.07.068.

[3] Cui, Z. Y., Guo, X. B., Yang, Q. X., Zhao, X., Qi, B. Q. (2018). Effects of roasted tobacco well-cellar transplanting on temperature, root vigor, growth and development, and yield quality in well-cellar. *Anhui Agricultural Science Bulletin*. 38-39+64. DOI: 10.16377/j.cnki.issn1007-7731.2018.14.018.

[4] Fan, Y. Y., Li, J. H., Yao, J. (2019). Research on a self-propelled tobacco transplanter. *Anhui Agricultural Science Bulletin*. 2019, 25, 121-122. DOI: 10.16377/j.cnki.issn1007-7731. 21.044.

[5] Gao, W. J. (2018). Design and analysis of integrated digging and tree planting equipment. *Forestry Machinery & Woodworking Equipment*. 2018,46,12-16. DOI: 10.13279/j.cnki.fmwe.2018.0047.

[6] Gao, Z. C., Li, L. J., Yang, H. J., Zhu, Q., Zhou, Y., Min, S. H. (2015). Design and test of forward and reverse screw type soil amendment lime spreader. *Transactions of the Chinese Society of Agricultural Engineering*. 2015, 31. DOI: 10.11975/j.issn.1002-6819.2015.10.006.

[7] Giuseppe B., Itai E. (2020). The mechanics of brittle granular materials with coevolving grain size and shape[J]. *Proceedings of the Royal Society A*, 2021, 477(2249). DOI: 10.1098/RSPA.2020.1005.

[8] Guo, G. S., Gao, M. X., Guo, K. Q., Dang, G. R. (2003). Study of screw auger parameters of mounted hole digger on the basis of MATLAB. *Journal of Northwest A & F University (Natural Science Edition).* 3, 179-182. DOI: 10.13207/j.cnki.jnwafu.2003.03.042.

[9] He, Y. P. (2013). *Experimental design and analysis*; Chemical Industry Press: Beijing, China.

[10] Jiang, K. S. (1997). Study on the theory of trencher's bit ascension--debate on the critical speed of the bit. *Journal of Central South University of Forestry & Technology*. 3. DOI: 10.14067/j.cnki.1673-923x.1997.03.014

[11] Jin, C. (2022). Dynamics simulation and experimental investigation of earth auger bit-soil based on EDEM. Fujian, *Fujian Agriculture and Forestry University*. DOI: 10.27018/d.cnki.gfjnu.2022.000429.

[12] Li, Y. Y., Hu, C. R. (2005*). Experimental design and data processing*; Chemical Industry Press: Beijing, China, 2005.

[13] Li, Z. H., Luo, P. (2005). *SPSS for Windows Statistical Analysis Tutorial*; Electronic Industry Press: Beijing, China, 2005.

[14] Liu, G. H., Yu, L. H., Chen, X., Zhang, F. G., Fu, D. L., Huang, H. G., Wu, X. M. (2018). Design and experiment of knapsack deep planting hole forming machine for large den. *Jiangsu Agricultural Sciences*, 46, 263-267. DOI: 10.15889/j.issn.1002-1302.2018.21.066.

[15] Liu, Z. C., Jiao, A. S., Jin, H. J. (2022). Structural design and test of auger crusher of 5TH shellless gourd seed picker. *Journal of Machine Design*. 39, 119-122. DOI: 10.13841/j.cnki.jxsj.2022.08.003.

[16] Lu, C. L. (2015). *Research and design of tobacco transplanting machine*; Jiangxi Agricultural University. 2015.

[17] Meng, Q. H. (2007). *Research on simulation and mathematical interpretation of dynamic process to earth auger for tree deep planting*. Northeast Forestry University.

[18] Qin, K., Ding, W. M., Fang, Z. C., Du, T. T., Zhao, S. Q., Wang, Z. (2016). Design and experiment of plowing and rotary tillage combined machine. *Transactions of the Chinese Society of Agricultural Engineering*. 2016, 32, 7-16. DOI: 10.11975/j.issn.1002-6819.2016.16.002.

[19] Song, Z. H., Li, H., Yan, Y. F., Tian, F. Y., Li, Y. D., Li, F. D. (2022). Calibration method of contact characteristic parameters of soil in mulberry field based on unequal-diameter particles DEM theory. *Transactions of the Chinese Society for Agricultural Machinery*. 2022,53,21-33. DOI: 10.6041/j.issn.1000-1298.2022.06.002.

[20] Sun, J. B., Liu, Q., Yang, F. Z., Liu, Z. J., Wang, Z. (2022). Calibration of discrete element simulation parameters of sloping soil on loess plateau and its interaction with rotary tillage components. *Transactions of the Chinese Society for Agricultural Machinery*. 2022, 53, 63-73. DOI: 10.6041/j.issn.1000-1298.2022.01.007.

[21] Tekeste, Z. M., Balvanz, R. L., Hatfield, L. J., Ghorbani, S. (2018). Discrete element modeling of cultivator sweep-to-soil interaction: Worn and hardened edges effects on soil-tool forces and soil flow [J]. *Journal of Terramechanics*, 2019, 82. DOI: 10.1016/j.jterra.2018.11.001.

[22] Wang, F. F., Xu, R., Wang, B., Yang, J., Liu, L., Yang, Y.J., Yu, H. Y. (2010). Advantages and main technologies of standardized cultivation of roasted tobacco under the film. *Modern Agricultural Science and Technology*. 5, 52. DOI: 10.3969/j.issn.1007-5739.2010.05.031.

[23] Xiao, W. B. (2010). *Design and experimental study of tobacco transplanting machine*; Hunan Agricultural University.

[24] Xiong, J., Yang, Y. F., Pan, X. F., Yuan, F. X., Fang, G. (2020). Design of tobacco transplant duckbill digging machine. *China Southern Agricultural Machinery*. 51, 78-79+84. DOI: 10.3969/j.issn.1672-3872.2020.15.033.

[25] Yang, W. W., Fang, L. Y., Luo, X. W., Li, H., Ye, Y. Q., Liang, Z. H. (2020). Experimental study of the effects of discharge port parameters on the fertilizing performance for fertilizer distribution apparatus with screw. *Transactions of the Chinese Society of Agricultural Engineering*. 36(17):1-8.

[26] Yao, R. K. (2017). *Study on the key technology of pit type transplanting in Flue-cured Tobacco*. Hunan Agricultural University.

[27] Yu, L. H., Liu, G. H., Zhang, F. G., Wu, X. M., Hu, C. S. (2018). Test and analysis for performance on the knapsack well-cellar making machine for seeding transplanting. *Journal of Agricultural Mechanization Research*. 40, 141-145. DOI: 10.13427/j.cnki.njyi.2018.03.028.

[28] Zheng, S. H., Jiang, F. H. (2004). *Experimental design and data processing*; China Building Materials Industry Press: Beijing, China.

[29] Zhuang, C. Q., Wu, Y. S. (1992). *Fundamentals of Applied Mathematical Statistics*; South China University of Technology Press: Guangzhou, China.